

Electron localization in a model polymer

S. Stafström, R. Riklund, and K. A. Chao

Department of Physics and Measurement Technology, University of Linköping, Linköping, Sweden

(Received 9 December 1981)

An unrestricted Hartree-Fock self-consistent numerical investigation on a model polymer represented by a stereo-irregular chain shows that the physical-disorder effect is weak even though the geometrical disorder is very strong. The regional and the global electron-localization lengths are studied via the inverse participation ratio and the moment analysis. In this system profound disorder effect appears when the system is anti-ferromagnetic.

Theoretical investigations on one-dimensional systems have followed several approaches with emphases on different aspects. The single-particle localization in a random potential of whatever origin is usually handled with simplified model Hamiltonians. The most extensively used Hamiltonian is the Anderson-type Hamiltonian. With certain approximations, the density of states and the main features of single-particle localization can be derived qualitatively.¹⁻⁴ Accurate quantitative results for physical properties can only be obtained by either the numerical calculation⁵ or the Monte Carlo method.⁶ On the other hand, the ground-state properties such as the cohesive energy and the equilibrium distance of realistic chain systems have been studied with the Hartree-Fock,⁷⁻¹¹ the SCF-LCAO,¹²⁻¹⁶ the extended-Hückel,¹⁷⁻¹⁹ the crystal orbital,²⁰ the coherent-potential approximation,²¹ and the band-structure calculation²² methods. These calculations have recently been reviewed by Andre.²³

A simple one-dimensional model which is sufficiently complex to reflect to certain extent the general properties of realistic systems and yet mathematically tractable is a periodic straight chain of hydrogen atoms. This model has earlier been investigated by many authors.²⁴⁻³⁰ However, a stereo-irregular chain of hydrogen atoms (SICHA) has not been much studied, although it is a suitable model for studying the disorder effect. Moreover, the SICHA simulates the geometric structure of many polymers. Consequently, characteristic features associated particularly to the stereo-irregular geometry are expected to be relevant to the general properties of polymers. The sophisticated theory of soliton has provided much insight of the conducting polymers. We will not refer to such work since the present numerical

study on the SICHA falls into another branch of interest.

A SICHA can be easily generated by a computer. Let us assume a Cartesian coordinate system $x_1-y_1-z_1$ and consider only the upper-half space with $z_1 \geq 0$. Taking the z_1 axis as the symmetry axis, we construct a right circular cone of angle θ_m with its tip at the origin. A vector \vec{R}_1 (drawn from the origin) within this cone can be represented by the polar coordinates (R_0, θ_1, ϕ_1) , where R_0 , θ_1 , and ϕ_1 are measured with respect to the $x_1-y_1-z_1$ system. Next, we consider a new Cartesian coordinate system $x_2-y_2-z_2$ with its origin at \vec{R}_1 and its positive z_2 axis in the direction of \vec{R}_1 . In the upper-half space of this new coordinate system an exact copy of the cone is constructed. Within this new cone, the second vector $\vec{R}_2-\vec{R}_1$ (\vec{R}_2 is also drawn from the origin of the $x_1-y_1-z_1$ system) can be similarly represented by the polar coordinates (R_0, θ_2, ϕ_2) , where R_0 , θ_2 , and ϕ_2 are measured with respect to the $x_2-y_2-z_2$ system. Again we consider a new Cartesian coordinate system $x_3-y_3-z_3$ with its origin at \vec{R}_2 and its positive z_3 axis in the direction of $\vec{R}_2-\vec{R}_1$. In the upper-half space of this new coordinate system a third same cone is constructed. Within this third cone, the third vector $\vec{R}_3-\vec{R}_2$ (\vec{R}_3 is also drawn from the origin of the $x_1-y_1-z_1$ system) can be again represented by the polar coordinates (R_0, θ_3, ϕ_3) , where R_0 , θ_3 , and ϕ_3 are measured with respect to the $x_3-y_3-z_3$ system. We continue this procedure repeatedly until N vectors $\{\vec{R}_i; i=1, N\}$ are generated. The positions of these N vectors are represented by R_0 and two sets of angles $\{\theta_i; i=1, N\}$ and $\{\phi_i; i=1, N\}$, when measured with respect to the proper coordinate systems. By generating a set of random numbers for these angles under the condi-

tions $0 \leq \theta_i \leq \theta_m$ and $0 \leq \phi_i < 2\pi$, and then attaching a hydrogen atom at each $\bar{\mathbf{R}}_i$, a SICHA of bond length R_0 and maximum tilt angle θ_m (corresponding to a minimum bond angle $\pi - \theta_m$) is then obtained. To avoid ambiguity, we use the terminology "a SICHA of zero degree" for a straight periodic chain ($\theta_m = 0$). It will be helpful to mention that the probability for a SICHA to doubling back on itself is negligibly small even for $\theta_m = \pi/6$ and $N = 62$. We have generated numerous SICHA with $N = 62$ and $\theta_m = \pi/6$, and found that the projected lengths of all these SICHA along the z_1 axis (from now on we will drop the subscript and name it as z axis) are about 80% to 90% of the total length NR_0 .

The Hamiltonian of a single SICHA is simply

$$H = \sum_i p_i^2/2m + \sum_i V^{\text{ion}}(\bar{\mathbf{r}}_i) + \frac{1}{2} \sum_{i,j} V^{e-e}(\bar{\mathbf{r}}_i - \bar{\mathbf{r}}_j), \quad (1)$$

where $V^{\text{ion}}(\bar{\mathbf{r}}_i)$ is the total ionic potential for the i th electron. The Coulomb interaction between the i th and j th electrons is $V^{e-e}(\bar{\mathbf{r}}_i - \bar{\mathbf{r}}_j)$, and the summations are over all the N electrons in a single SICHA. The Hamiltonian will be solved with the unrestricted Hartree-Fock approximation with a modification of the spin-polarized potential. This method has been formulated and discussed in details for the randomly distributed shallow impuri-

ties in semiconductors.³¹ Here we will only briefly outline the key points. Let $\phi_i(\bar{\mathbf{r}}) \equiv \phi(\bar{\mathbf{r}} - \bar{\mathbf{R}}_i)$ be the hydrogen $1s$ wave function centered at the i th atom, and the single-particle eigenfunction of the unrestricted Hartree-Fock equation be constructed as

$$\Psi_{i\sigma}(\bar{\mathbf{r}}) = \sum_j \phi_j(\bar{\mathbf{r}}) B_{\sigma ji}. \quad (2)$$

Then the unrestricted Hartree-Fock approximation leads to two coupled equations for both spin $\sigma = \uparrow$ and \downarrow

$$\tilde{B}_\sigma^\dagger \tilde{H}_{0\sigma} \tilde{B}_\sigma = \tilde{E}_\sigma, \quad (3)$$

where \tilde{B}_σ is the matrix of the coefficients $B_{\sigma ij}$ and \tilde{E}_σ is the diagonal Hartree-Fock eigenenergy matrix for the spin σ . We define $N(\sigma)$ as the number of σ -spin electrons in the SICHA and $\Gamma(\sigma)$ as the set of indices which specifies the $N(\sigma)$ single-particle eigenfunctions occupied by the σ -spin electrons. The matrix elements of $\tilde{H}_{0\sigma}$ can now be expressed as

$$H_{0\sigma ij} = \int \phi_{i\sigma}^*(\bar{\mathbf{r}}) [p^2/2m + V^{\text{ion}}(\bar{\mathbf{r}})] \phi_{j\sigma}(\bar{\mathbf{r}}) d\bar{\mathbf{r}} + \sum_s \sum_{l \in \Gamma(s)} [\tilde{B}_\sigma^\dagger \tilde{V}(\sigma s : ij) \tilde{B}_\sigma]_{ll}, \quad (4)$$

where the electron-electron interaction matrix is defined as

$$V(\sigma s : ij)_{iq} = \int \int \phi_{i\sigma}^*(\bar{\mathbf{r}}) \phi_{is}^*(\bar{\mathbf{r}}') V^{e-e}(\bar{\mathbf{r}}' - \bar{\mathbf{r}}) [\phi_{qs}(\bar{\mathbf{r}}') \phi_{j\sigma}(\bar{\mathbf{r}}) - \phi_{qa}(\bar{\mathbf{r}}) \phi_{j\sigma}(\bar{\mathbf{r}}') \delta_{s\sigma}] d\bar{\mathbf{r}} d\bar{\mathbf{r}}'. \quad (5)$$

In the limit of very large R_0 the energy spectrum of (3) consists of only two delta functions $\delta(E - E^0)$ and $\delta(E - E^-)$. E^0 is the ionization energy of a neutral hydrogen and E^- is the ionization energy of a negatively charged hydrogen H^- . However, if we use the form (5) and solve (3) self-consistently by iteration, we find that H^- is not stable in contradiction to the experimental finding. This is due to the neglect of the electron correlation effect when two electrons of opposite spins occupy the same atom. Therefore, for H^- one should replace the product-function $\phi_{i\uparrow}(\bar{\mathbf{r}}_1) \phi_{i\downarrow}(\bar{\mathbf{r}}_2)$ by a two-particle wave function $\Phi_i(\bar{\mathbf{r}}_1, \bar{\mathbf{r}}_2)$. Chandrasekhar obtained such a two-particle wave function a long time ago which yields a very accurate ionization energy of H^- .³² We will use the Chandrasekhar wave function in the present calculation, and the calculation details are the same as in the previous work on doped semiconductors.³¹

Since the ferromagnetic phase is very unlikely to be stable in a SICHA, we have set $N(\uparrow) = N(\downarrow) = N/2$ in our calculation to investigate two cases: 0-SICHA for $\theta_m = 0$ and 30-SICHA for $\theta_m = \pi/6$. For both cases the number of atoms N in the SICHA is 62. For convenience, we use the atomic unit with energy in Hartree. The disorder effect on the density of states has already been reported elsewhere.³³

Let S be a path starting from the origin, passing through the hydrogen sites at the positions $\bar{\mathbf{R}}_1, \bar{\mathbf{R}}_2, \bar{\mathbf{R}}_3, \dots$, and then ending at $\bar{\mathbf{R}}_{62}$. Between $\bar{\mathbf{R}}_i$ and $\bar{\mathbf{R}}_{i+1}$ the path follows a straight line. Hence the total length of S is just NR_0 . Along this path we define two spin-density functions $\rho_\sigma(r)$ as

$$\rho_\sigma(r) = \sum_{i=1}^{31} |\Psi_{i\sigma}(r)|^2, \quad \sigma = \uparrow, \downarrow \quad (6)$$

where r is measured along S with $r = 0$ at the ori-

gin. We should notice that in (6) the summation runs over only the occupied eigenstates which form the lower half of the eigenenergy spectrum. In our notation the 62 eigenstates for each spin are labeled by i from 1 to 62 with increasing eigenenergy. For the case of 0-SICHA, S is along the positive z axis and the spatial density of electrons is cylindrically symmetric with respect to S . Therefore, the variation of the spin density along the 0-SICHA can be demonstrated better by the total spin density

$$\rho_{\sigma}^*(r) = \int_{A(r)} \left[\sum_{i=1}^{31} |\Psi_{i\sigma}(\vec{r})|^2 \right] da, \quad (7)$$

where the domain $A(r)$ of the surface integration is an infinite plane intersecting the path S at r perpendicularly. However, $\rho_{\sigma}^*(r)$ is not a good measure of the spin density along the 30-SICHA because two planes $A(r)$ and $A(r')$ are not necessarily parallel. Consequently, we will calculate $\rho_{\sigma}(r)$ for both the 0-SICHA and the 30-SICHA in order to investigate the effect of disorder on magnetic ordering.

The $\rho_{\sigma}(r)$ for the 0-SICHA with $R_0 = 2-8$ (in units of Bohr radius) are shown in Fig. 1. The values of R_0 are marked by the numbers at the right-hand side. The horizontal axis r/R_0 labels the position along the path S such that integer values of r/R_0 represent the hydrogen sites. For each value of R_0 the vertical scale at the left-hand side consists of two parts: The upper scale is for $\rho_{\uparrow}(r)$ and the lower one is for $\rho_{\downarrow}(r)$. We would like to remind the reader that $\rho_{\sigma}(r)$ is non-negative. Hence, for each R_0 the curves $\rho_{\uparrow}(r)$ and $\rho_{\downarrow}(r)$ do not intersect each other. When R_0 is large, Fig. 1 indicates that the 0-SICHA is antiferromagnetic. The antiferromagnetic structure gradually disappears when $R_0 \rightarrow 2$. It will be helpful to elaborate the cases of $R_0 > 5$ which exhibit almost complete antiferromagnetic order along the path S . For $R_0 > 5$, $\rho_{\sigma}(r)$ can be well approximated as

$$\rho_{\sigma}(r) \simeq \sum_{j=1}^{62} \left[\sum_{i=1}^{31} |B_{\sigma ji}|^2 \right] \phi_j^2(r).$$

If we take $R_0 = 6$ and let r_{\uparrow} be the position of an up-spin site, then we have

$$\rho_{\uparrow}(r_{\uparrow} + R_0) / \rho_{\uparrow}(r_{\uparrow}) \simeq \exp(-R_0) = 0.00247.$$

Before we present the result of $\rho_{\sigma}(r)$ for the 30-SICHA, it is necessary to analyze the electronic energies first. The electronic energies in a SICHA can be separated into three classes. The first class is the intra-atomic Coulomb energy between two electrons occupying the same atomic orbital. The

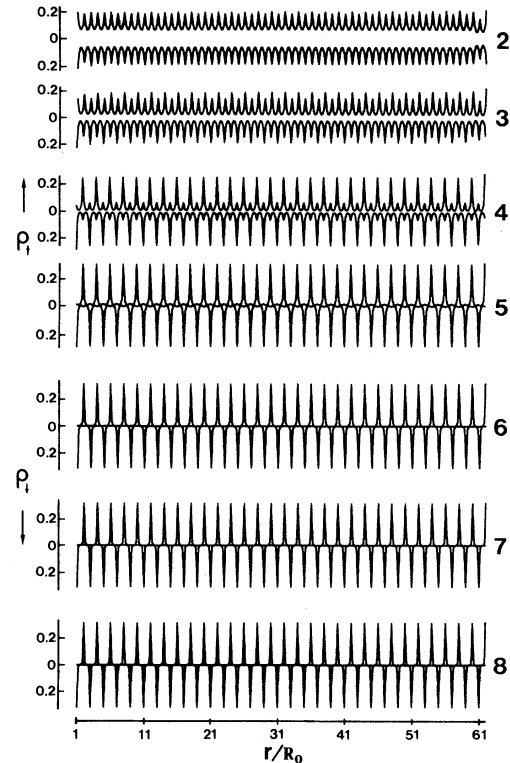


FIG. 1. Spin-density distribution along the center line of a 0-SICHA for various values of R_0 marked at the right-hand side. For each R_0 at the left-hand side the upper scale is for $\rho_{\uparrow}(r)$ and the lower scale is for $\rho_{\downarrow}(r)$. R_0 is in units of Bohr radius.

nearest-neighbor electron hopping energy and the nearest-neighbor Coulomb and exchange energies between electrons form the second class. The third class consists of the far-neighbor hopping and the far-neighbor electronic Coulomb and exchange energies. Let ϵ_1 , ϵ_2 , and ϵ_3 represent the first, second, and third classes of energies, respectively. For large value of R_0 , the ratios ϵ_2/ϵ_1 and ϵ_3/ϵ_2 decrease exponentially with R_0 . The magnetic coupling strength J which stabilizes the antiferromagnetic phase for large value of R_0 is of order ϵ_2^2/ϵ_1 .

Because of the constant nearest-neighbor distance R_0 in a SICHA, the disorder effect in a 30-SICHA is due to the fluctuation $\delta\epsilon_3$ of the energy ϵ_3 . Such fluctuation is very small compared to ϵ_2 and extremely small compared to ϵ_1 . However, $\delta\epsilon_3$ and J are of the same order of magnitude. Therefore, when the antiferromagnetic phase in a 0-SICHA is stable, the characteristic feature of the single-particle eigenstate $\Psi_{i\sigma}(\vec{r})$ will be altered drastically by the disorder effect. On the other

hand, the fact $\epsilon_1 \gg \delta\epsilon_3$ prevents the transfer of spins from one sublattice to the other when the 0-SICHA is changed to the 30-SICHA. Hence, as the very weak disorder effect is introduced into the antiferromagnetic phase of the 0-SICHA, there is only a charge redistribution within the same sublattice but without spin flip. At the other limit of small R_0 the properties of the single-particle eigenstates are dominated by ϵ_1 and ϵ_2 which are much greater than $\delta\epsilon_3$. In this case the change of the eigensolutions of (3) due to $\delta\epsilon_3$ is then negligibly small. Let us recall that $\rho_\sigma(r)$ is the total spin density over all the occupied eigenstates. Consequently, for any value of R_0 we expect an extremely small difference in $\rho_\sigma(r)$ between the case 0-SICHA and the case 30-SICHA. This is indeed correct since there is no difference (within the accuracy of the drawing) between Fig. 1 and the similar plot for the 30-SICHA.

In order to demonstrate the effect of $\delta\epsilon_3$ on the single-particle eigenstates, let us define the inverse participation ratio (\mathcal{R}) of the i th eigenstate with σ spin as

$$\mathcal{R}_{\sigma i} = \left[\sum_j |B_{\sigma ji}|^4 \right] / \left[\sum_j |B_{\sigma ji}|^2 \right]^2. \quad (8)$$

If the atomic orbitals $\phi_i(\vec{r})$ are orthogonal to each other and the system is infinite, then the value of $\mathcal{R}_{\sigma i}$ varies from zero for extremely extended states to one for extremely localized states. Although in our case these two conditions are not satisfied, we can still use the \mathcal{R} to estimate the degree of localization. For given values of $R_0 = 1.5$ and 2–5, the $\mathcal{R}_{\sigma i}$ of both $\sigma = \uparrow$ and $\sigma = \downarrow$ are given in Fig. 2(a) (for 0-SICHA) and Fig. 2(b) (for 30-SICHA). For each value of R_0 there is a particular coordinate system attached to the associated \mathcal{R} data. The values of R_0 are marked by the numbers above the vertical axes. The horizontal axes in these figures label the eigenenergies of the single-particle eigenstates $\psi_{i\sigma}(\vec{r})$. The $\mathcal{R}_{\sigma i}$ of each eigenstate is represented by a dot. The scales for both the vertical and the horizontal axes are given at the lower-left corner with E in unit of Hartree. The eigenenergy spectrum for a fixed value of R_0 can be clearly divided into two parts, as a result of the intra-atomic Coulomb interaction (ϵ_1) between electrons. To avoid ambiguity, we call them the lower Coulomb-split spectrum (LCSS) and the upper Coulomb-split spectrum (UCSS). For small value of R_0 , for example, $R_0 = 1.5$ and 2, some eigenstates in the UCSS have very large \mathcal{R} . This is due to the intrinsic drawback of the Hartree-Fock ap-

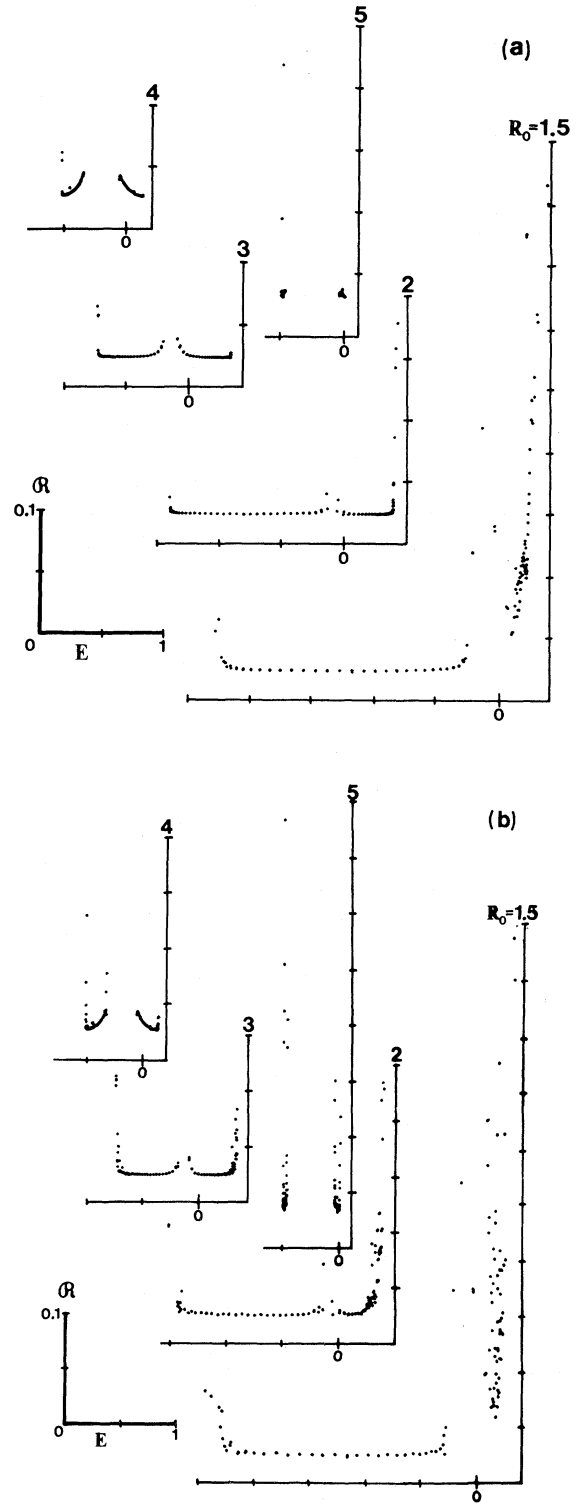


FIG. 2. Inverse participation ratio (for both \uparrow and \downarrow spins) as a function of eigenenergy for various values of R_0 marked at the top of the corresponding vertical axis. The scales for the axes are given at the lower-left corner. (a) for 0-SICHA and (b) for 30-SICHA.

proximation which has been discussed earlier in connection to the density of states.³³ Since for the ground state the UCSS is always empty, we can ignore it for the moment. The slight increase of \mathcal{R} at both ends of the LCSS is associated to the boundary condition for a finite chain. In general, the values of \mathcal{R} in Fig. 2(a) are very small, indicating the bandtype eigenstates.

We notice that in Fig. 2(a), as R_0 increases the shape of the \mathcal{R} associated to the LCSS changes from very flat (for example, $R_0=1.5$) to more curved (for example, $R_0=4$) and to flat again (for example, $R_0=5$). This is caused by the gradual increase of the antiferromagnetic ordering. To illustrate this point, in Fig. 3 the \mathcal{R} of the almost complete antiferromagnetic cases $R_0=6-8$ are shown at the left, the middle, and the right, respectively. The result for each R_0 consists of two parts: The group of dots at the upper part is for the 30-SICHA and the group of dots at the lower part is for the 0-SICHA. The few star-points mixing with the dots of the upper group are also for the 0-SICHA. However, the large \mathcal{R} values of these few star points are the results of the boundary conditions for a finite chain and will be ignored. The scale of energy for the horizontal axes associated to

a particular value of R_0 is plotted above the corresponding dot data. For each value of R_0 , the vertical axis at the left is for the 30-SICHA and that at the right is for the 0-SICHA. For such large R_0 the eigenstates of the 0-SICHA are the sublattice Bloch states and the energy spectrum is of the type of an antiferromagnetic split band. Hence the \mathcal{R} values are very small. Because of the antiferromagnetic structure, both the UCSS and the LCSS are again split into two magnetic subspectra. In Fig. 3 a gap between the magnetic subspectra of the UCSS can be clearly detected, but the gap in the LCSS is too small to be seen. When R_0 is very small, the eigenstates of the 0-SICHA are the pure Bloch states without sublattice structure. Consequently, as R_0 increases the single-particle eigenfunctions of the 0-SICHA change from the pure Bloch type through the non-Bloch type to the sublattice Bloch type. This explains the variation of the shape of \mathcal{R} for the 0-SICHA when R_0 increases from 1.5 to 5 [Fig. 2(a)] and to 8 (Fig. 3).

When the disorder effect is introduced, by comparing the data for the 0-SICHA and the 30-SICHA in Figs. 2(a), 2(b), and 3, we see that band tails appear at both sides of the LCSS and the UCSS. The extent of band-tailing grows with the extent of antiferromagnetic ordering. The states in

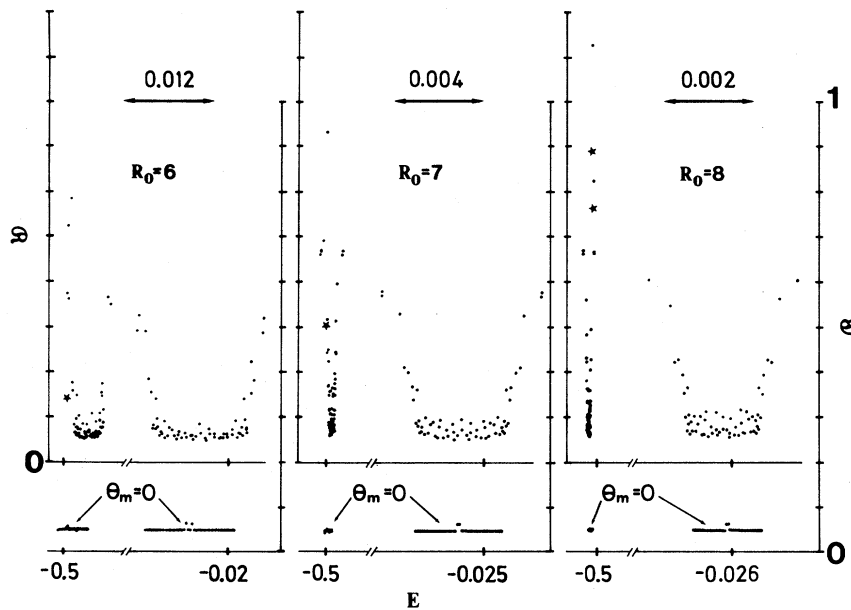


FIG. 3. Inverse participation ratio (for both \uparrow and \downarrow spins) as a function of eigenenergy for $R_0=6$ (left plot), 7 (middle plot), and 8 (right plot). The upper group of dots is for 30-SICHA, and the lower group of dots plus the star points are for the 0-SICHA. The left vertical axis is for the 30-SICHA and the right vertical axis is for the 0-SICHA. For each R_0 the scale of energy for the horizontal axis is given at the top of the figure.

the tails are more localized, as indicated by the larger \mathcal{R} values. With decreasing R_0 the antiferromagnetic structure gradually disappears, and so the disorder effect gets weaker as we pointed out earlier. Therefore, in Figs. 2(a), 2(b), and 3 we see that the difference between the \mathcal{R} of the 0-SICHA and the 30-SICHA becomes less as the nonmagnetic phase is approached.

Let us consider a localized state

$$\Psi_{\sigma i}(\vec{r}) = \sum_{j=1}^{\nu} \phi_j(\vec{r}) B_{\sigma j i}$$

such that ν of the coefficients, for example, $j = \xi_1, \xi_2, \dots, \xi_\nu$ are much larger than the rest of the coefficients. Hence the state $\Psi_{\sigma i}(\vec{r})$ is localized on a set of atoms at $\{\vec{R}_{\xi_j}; j = 1, \nu\}$. However, the spatial distribution of the atomic positions $\{\vec{R}_{\xi_j}; j = 1, \nu\}$ does not change the value of $\mathcal{R}_{\sigma i}$. If all these ν atomic positions are very close to each other, then the envelope function of $B_{\sigma j i}$, denoted as $F_{\sigma i}(\vec{r} - \vec{\tau})$, has only one maximum around $\vec{\tau}$. In terms of the envelope function we can define a *regional localization length* ξ_i . However, it is possible that these ν atomic positions $\{\vec{R}_{\xi_j}; j = 1, \nu\}$ form μ spatially separated regions such that only the atomic positions within the same region are close to each other. Then the envelope function has the form

$$\sum_{k=1}^{\mu} F_{\sigma i k}(\vec{r} - \vec{\tau}_k)$$

with μ local maxima around $\{\vec{\tau}_k; k = 1, \mu\}$. Although around each local maximum a *regional localization length* ξ_{ik} can be still defined, we need a *global localization length* Ξ_i which measures the largest distance between two regions. To avoid ambiguity, we call the localization of $\Psi_{\sigma i}(\vec{r})$ a *pure regional localization* if $\mu = 1$, but a *global localization* if $\mu > 1$.

Certainly, the \mathcal{R} can not tell the difference between the global localization and the pure regional localization. On the other hand, the moments defined as

$$L_m^\sigma(i) = \frac{1}{Z} [\langle \Psi_{\sigma i}(\vec{r}) | (z - \langle z \rangle)^m | \Psi_{\sigma i}(\vec{r}) \rangle]^{1/m}, \quad m \geq 2 \quad (9)$$

gives valuable information about the characteristic feature of the localization properties, where $Z = |(\vec{R}_{62} - \vec{R}_1) \cdot \hat{z}|$ is the projected length of the SICHA along the z axis. For $R_0 = 1.5, 4, \text{ and } 7$, the five moments $L_m^\downarrow(i)$ with $m = 2-6$ are shown in Figs. 4(a)–4(c). Each moment is plotted in one

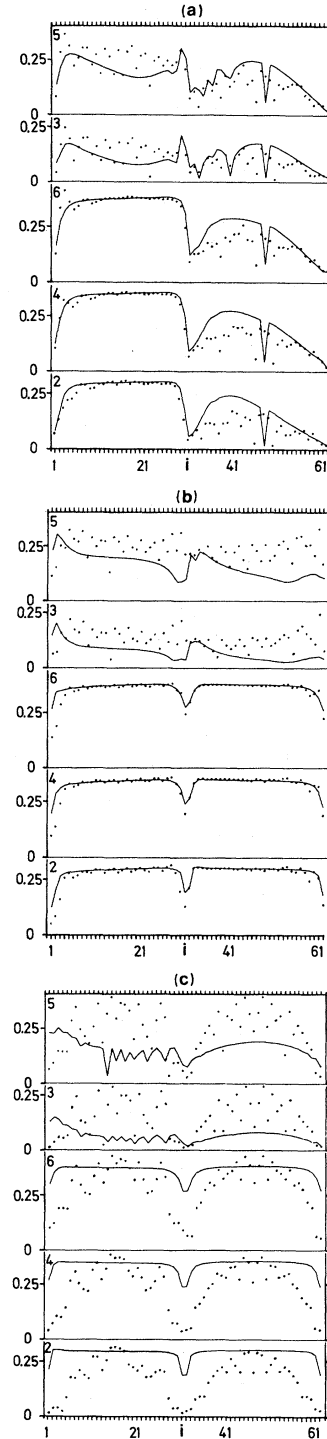


FIG. 4. Moments for down-spin eigenstates [$L_m^\downarrow(i)$ for even moments $m = 2, 4, \text{ and } 6$ but $|L_m^\downarrow(i)|$ for odd moments $m = 3 \text{ and } 5$] with the solid curves for the 0-SICHA and the dots for the 30-SICHA. Each panel is for one moment with the number m marked at the upper-left corner. Horizontal axis labels the eigenstates with increasing eigenenergy. (a) for $R_0 = 1.5$, (b) for $R_0 = 4$, and (c) for $R_0 = 7$.

panel with the value of m marked at the upper-left corner. Since the odd moments fluctuate randomly between the positive and the negative values, we found it better to plot the absolute values of the odd moments $|L_{3}^{\downarrow}(i)|$ and $|L_{5}^{\downarrow}(i)|$. The horizontal axis labels the eigenstate quantum number with increasing eigenenergy. In these figures, the solid curves are for the 0-SICHA and the dots are for the 30-SICHA. The moments for the up-spin eigenstates are not shown here because they are very similar to those for the down spin.

Since the disorder effect is weak for small R_0 , the even moments of the 0-SICHA and the 30-SICHA, which measure the degree of localization, in Figs. 4(a) and 4(b) are almost the same. Here again we ignore the unusual feature of the moments associated to the UCSS of $R_0=1.5$ for the same reason mentioned earlier. When the disorder effect is introduced, we see a general increase of the absolute values of the odd moments. The eigenstates of the 30-SICHA are thus more asymmetric than those of the 0-SICHA. Nevertheless, as far as the electron localization is concerned, the moment analysis and the \mathcal{R} calculation provide the same information.

However, it is not so for $R_0=7$ where the disorder effect is very strong. The \mathcal{R} data in Fig. 3 suggest the existence of a few localized states only in the band tails, while all the states in the bulk part of the spectrum are delocalized. In Fig. 4(c) the even moments for the 30-SICHA have broad peaks at the centers of both the LCSS and the UCSS. Around the peaks the moments of both the

0-SICHA and the 30-SICHA have roughly the same value. Hence, these eigenstates of the 30-SICHA are localized in the sense of the global localization (if the global localization length is sufficiently long we can also say that the state is delocalized in non-Bloch type). Moving away from these peak areas, the global localization gradually changes into the pure regional localization as indicated by the decreases of the even moments. Since we know the numerical values of $B_{\sigma ji}$ for all the eigenstates we can check the characteristic feature of the localization properties of the eigenstate. We found that almost all the eigenstates in the bulk parts of both the UCSS and the LCSS have a substantial number of large coefficients $B_{\sigma ji}$. But the spatial distribution of these $B_{\sigma ji}$ varies from the global localization type for some states to the pure regional localization type for some other states. Of course, such change of spatial distribution can not be detected by the \mathcal{R} calculation. In the tails of the spectra, the localization is indeed pure regional.

To close up, we should stress that the finding in this paper is characteristic to the geometric property of a stereo-irregular chain, independent of the use of hydrogen wave function. Namely, as long as the bond length R_0 is constant and the disorder is due to the random variation of the bond angle, the physical disorder effect is weak (except for the antiferromagnetic phase), even though the topological disorder may be rather large. For the antiferromagnetic phase, the disorder energy is not strong enough to localize all the electrons in pure regional type.

-
- ¹J. C. Kimball, J. Phys. C **11**, 1367 (1978).
²R. Day and F. Martino, J. Phys. C **14**, 4247 (1981).
³V. M. Koleshko and N. Yu. Trifonov, Phys. Status Solidi B **104**, K105 (1981).
⁴F. Tanaka, Prog. Theor. Phys. **65**, 751 (1981).
⁵R. C. Albers and J. E. Gubernatis, Phys. Rev. B **17**, 4487 (1978).
⁶P. M. Richards and R. L. Renken, Phys. Rev. B **21**, (1980).
⁷A. Karpfen and P. Schuster, Chem. Phys. Lett. **44**, 459 (1976).
⁸R. A. Harris and L. M. Falicov, J. Chem. Phys. **51**, 5034 (1969).
⁹M. Kertesz, Phys. Status Solidi B **69**, K141 (1975).
¹⁰A. Karpfen, J. Phys. C **12**, 3227 (1979).
¹¹J. Delhalle, L. Piela, J.-L. Bredas, and J. M. Andre, Phys. Rev. B **22**, 6254 (1980).
¹²G. Del Re, J. Ladik, and G. Biczko, Phys. Rev. **155**, 997 (1967).
¹³J. M. Andre, J. Chem. Phys. **50**, 1536 (1969).
¹⁴M. Kertesz, J. Koller, A. Azman, and S. Suhai, Phys. Lett. **55A**, 107 (1975).
¹⁵C. Merkel and J. Ladik, Phys. Lett. **56A**, 395 (1976).
¹⁶J. Ladik and M. Seel, Phys. Rev. B **13**, 5338 (1976).
¹⁷R. Hoffmann, J. Chem. Phys. **39**, 1397 (1963).
¹⁸J. Delhalle, J. M. Andre, S. Delhalle, J. J. Pireaux, R. Caudano, and J. J. Verbist, J. Chem. Phys. **60**, 595 (1974).
¹⁹M. Kertesz and G. Gondor, J. Phys. C **14**, L851 (1981).
²⁰A. Karffen, Chem. Phys. Lett. **64**, 299 (1979).
²¹M. Seel, *Recent Advances in the Quantum Theory of Polymers*, Vol. 113 of *Lecture Notes in Physics* (Springer, Berlin, 1979), p. 271.

- ²²W. L. McCubbin, *Chem. Phys. Lett.* **8**, 507 (1971).
- ²³J. M. Andre, *Adv. Quantum Chem.* **12**, 65 (1980).
- ²⁴J.-L. Calais, *Ark. Fys.* **28**, 511 (1965).
- ²⁵K.-F. Berggren and F. Martino, *Phys. Rev.* **184**, 484 (1969).
- ²⁶D. H. Kislow, J. M. McKelvey, C. F. Bender, and H. F. Schaefer, III, *Phys. Rev. Lett.* **32**, 933 (1974).
- ²⁷M. Kertesz, J. Koller, and A. Azman, *Phys. Rev. B* **14**, 76 (1976).
- ²⁸M. Kertesz, J. Koller, and A. Azman, *Theor. Chem. Acta* **41**, 89 (1976).
- ²⁹J. Delhalle and F. E. Harris, *Theor. Chem. Acta* **48**, 127 (1978).
- ³⁰R. S. Day, *Phys. Lett.* **85A**, 405 (1981).
- ³¹K. A. Chao, R. Riklund, and A. Ferreira da Silva, *Phys. Rev. B* **21**, 5745 (1980); for the correction with the Chandrasekhar wave function, see R. Riklund and K. A. Chao (unpublished).
- ³²S. Chandrasekhar, *Astrophys. J.* **100**, 176 (1944).
- ³³R. Riklund and S. Stafström (unpublished).